Numerical studies of antiferromagnetism on a Kagomé net

Chen Zeng and Veit Elser
Laboratory of Atomic and Solid State Physics, Cornell University, Ithaca, New York 14853-2501
(Received 28 June 1990)

We investigate the Heisenberg antiferromagnet with spins on a Kagomé net as recently proposed to explain an anomaly in the heat capacity of adsorbed ^{3}He. The model reveals a disordered ground state from our spin-wave calculation which is consistent with the results of the spin-spin correlation functions computed by direct diagonalization of small clusters. We also obtain evidence of a double-peak feature in the heat capacity using the decoupled-cell Monte Carlo simulation technique introduced by Homma *et al.*

I. INTRODUCTION

The study of nuclear spin ordering in multilayer ^{3}He films has been a stimulating subject for the last decade. A combination of techniques including NMR,[1,2] neutron scattering,[3] and heat-capacity measurements[4,5] has led to a fairly detailed description of the phase diagram of ^{3}He adsorbed on graphite. The second ^{3}He layer, in particular, can form a low-density solid with considerably larger exchange interactions than the highly compressed first layer on which it rests. Recently, heat-capacity measurements at millikelvin temperatures by Greywall and Busch[4] have revealed two mysterious facts: (1) The second-layer heat capacity shows a sharp peak at 2.5 mK and (2) the entropy change through this peak is only one-half of the expected $k_B \ln 2$ per second-layer spin. It is interesting to note that this experiment leaves little choice about the existence of another peak in the heat capacity below 2.5 mK to account for the missing entropy.

Various explanations of the double-peak anomaly in the second-layer heat capacity have been proposed.[6–8] One of us[6] exploited the likely registered structure of the low-density second-layer solid to obtain a nearest-neighbor Heisenberg antiferromagnet (HAF) spin Hamiltonian with two exchange constants. The double peak was claimed to arise when one exchange constant, which couples only spins on a Kagomé net (see Fig. 1), is much larger than the other. Meanwhile, Roger[7] has emphasized the role of multispin ring exchange processes and also finds a double peak in a finite-size cluster (16 spins) by tuning different exchange constants. A somewhat different approach, involving a nearly half-filled Hubbard model, was explored by Machida and Fujita.[8]

The motivation of the study presented in this paper is twofold. On the one hand, we wish to provide further evidence for the existence of a double peak in the heat capacity of the HAF on a Kagomé net. The HAF on a Kagomé net is interesting in its own right since it appears to be the first spin-$\frac{1}{2}$ model in two dimensions involving only nearest-neighbor interactions that shows a disordered ground state. As our second aim, we explore using spin-wave calculations the effect of coupling the spins of the Kagomé net to the remaining spins in the triangular ^{3}He lattice.

The paper is organized as follows: In Sec. II numerical diagonalization of clusters up to 21 spins are performed to obtain the ground-state energy, spin-spin correlation functions, and spin gap at zero temperature. In Sec. III we present a spin-wave calculation for a spin-$\frac{1}{2}$ triangular lattice with two couplings. Section IV deals with thermodynamical properties. We have used the decoupled cell Monte Carlo scheme introduced by Homma *et al.*[9] to show the double-peak feature. We end in Sec. V with our conclusions.

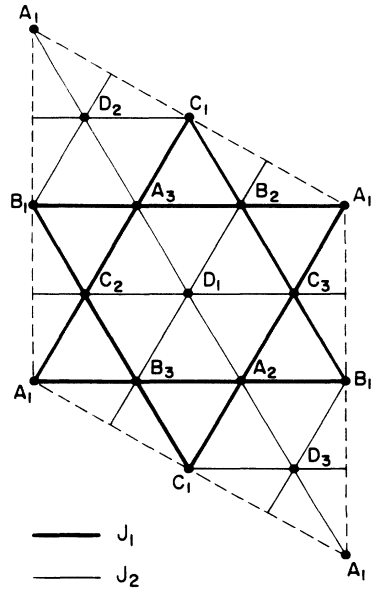

FIG. 1 Unit cell of the triangular lattice with two exchange constants J_1 and J_2. J_1 couples only spins on a Kagomé net (thick lines). The twelve sublattices A_λ, B_λ, C_λ, and D_λ are discussed in Sec. III.

II. DIAGONALIZATION OF FINITE CLUSTERS

We have obtained fairly direct numerical evidence that the spin-$\frac{1}{2}$ HAF on the Kagomé net has a disordered ground state by diagonalizing the Hamiltonian for small clusters. The Hamiltonian may be written in the form

$$H=J\sum_{\langle ij\rangle}\mathbf{S}_i\cdot\mathbf{S}_j\ , \tag{2.1}$$

where the $\mathbf{S}_i$ are the spin-$\frac{1}{2}$ operators, the sum is over nearest neighbors of a Kagomé net, and J has the positive sign for antiferromagnetism. Following Fujiki and Betts,[10,11] we used equilateral parallelograms with $N=9,12,15,21$ spins and a nonequililateral parallelogram with $N=18$ spins, all having periodic boundary conditions. These finite clusters are depicted in Fig. 2.

The Hamiltonian (2.1) commutes with each component of the uniform magnetization operator $\mathbf{M}$, and so the eigenvalue of

$$M^z=\sum_i S_i^z \tag{2.2}$$

has been chosen as a good quantum number where S_i^z is the z component of the ith spin. The orthonormal states denoted by $|S_1^zS_2^z\cdots S_N^z\rangle$ have been used as base states to generate matrix elements of the Hamiltonian. For the ground-state properties, we restrict ourselves to the subspace with the minimum magnetization M^z, i.e., $M^z=0$ for even-spin clusters and $M^z=\frac{1}{2}$ for odd-spin clusters.

For $N\leq 21$ we were able to diagonalize the Hamiltonian by using translational symmetries alone. The rank of the Hamiltonian to be diagonalized for $N=21$, for example, after using all seven translations is 50 388 for $M^z=\frac{1}{2}$ and 41 999 for $M^z=\frac{3}{2}$. The ground-state energy and wave function have been obtained by a simple iterative power method.

The ground-state energy per spin as a function of $1/N$ is plotted in Fig. 3. The data follow two different trends depending on whether N is even or odd. Only the odd-N values were used to perform a least-squares extrapolation for $N\rightarrow\infty$ because (1) there is one more data point and (2) the $N=18$ cluster forms a nonequilateral parallelogram unlike the others. The least-squares fit (solid line in Fig. 3) yielded

$$E_0/NJ=-0.434\pm0.002\ , \tag{2.3}$$

where the uncertainty was estimated by least-squares fits of various pairs of odd-N data. If, as we believe, the ground state has spin-Peierls order, i.e., broken translational symmetry, then the corrections to the ground-state energy would not scale smoothly with N but rather would reflect the commensurability of the magnetic unit cell with each cluster. In view of the small number of the data points, we have not pursued this form of analysis. It is worth noting that (2.3) is substantially lower than the exact upper bound $-\frac{5}{12}=-0.417\ldots$ given by Elser.[6]

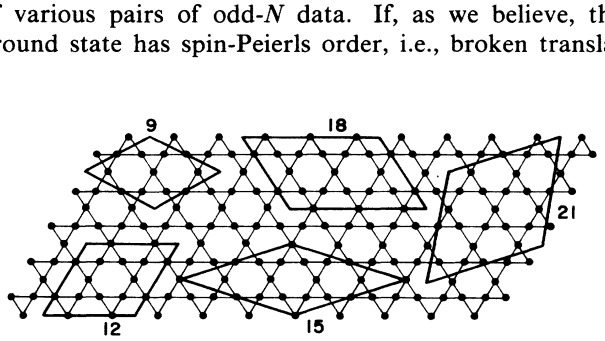

FIG. 2. Finite clusters used in the numerical diagonalizations.

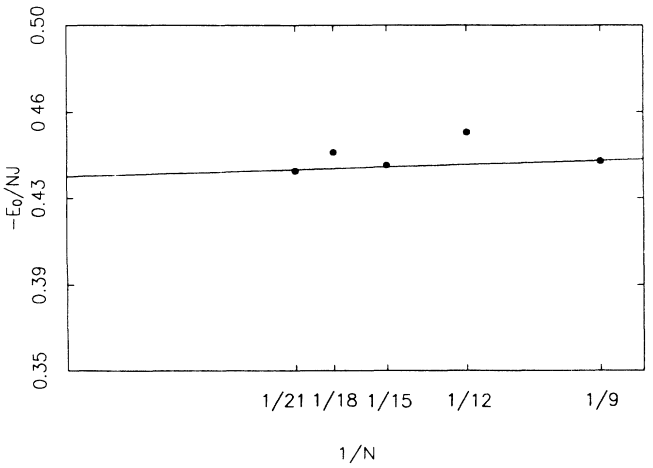

FIG. 3. Ground-state energy per spin as a function of the inverse cluster size. The data points correspond to $N=9$, 12, 15, 18, 21 from the right to the left. Only the odd-N data have been used for the least-squares fit (solid line) to extrapolate to the infinite size estimate -0.434.

Our results for the spin-spin correlations on the $N=21$ cluster are given in Table I. Since the $N=21$ cluster has a lower point-group symmetry than the infinite Kagomé net, we averaged the spin-spin correlation functions for spin pairs that become symmetry related in the infinite system, but are symmetry inequivalent in the cluster. When the signs of such spin pairs begin to fluctuate, we display the range of their values (last two rows in Table I). We identify spin pairs in terms of their separation: the Euclidean distance r as well as the minimum path length of bonds n connecting the two spins. The rapid decay of correlations with separation is especially striking when compared with the corresponding values on a triangular lattice given by Nishimori and Nakanishi (reproduced in Table I). While the spin correlations on the triangular lattice vary slowly, e.g., the second-nearest-neighbor value being about 95% of the nearest-neighbor value, the results on the Kagomé net reveal a dramatic

TABLE I. Spin-spin correlations in the 21-spin Kagomé cluster. The spacing of near neighbor spins is unity.

n (Path length)	r (Distance)	$\langle S_0^z\cdot S_n^z\rangle$ (Kagomé net)	$\langle S_0^z\cdot S_n^z\rangle$ (Triangular lattice) (Refs. 11 and 12)
1	1	−0.072 79	−0.062 32
2	$\sqrt{3}$	0.009 74	0.059 16
2	2	0.013 69	−0.025 56
3	2	−0.000 38 ~ −0.000 51	−0.025 56
3	$\sqrt{7}$	−0.015 43 ~ −0.019 57	0.032 88

TABLE II. Numerical diagonalization results for ground-state energy E_0 and spin-gap Δ.

N (System size)	E_0/NJ (Ground-state energy)	$\Delta=E_1-E_0$ (Spin gap)
9	−0.4410	0.6750
12	−0.4537	0.3827
15	−0.4393	0.4193
18	−0.4449	0.2451
21	−0.4368	0.2394

drop, i.e., the corresponding ratio becomes about 15%. This itself strongly suggests the possibility of a disordered ground state on the Kagomé net in contrast to the triangular lattice where the ground state is believed to have antiferromagnetic order with three sublattices. Indeed, this conclusion is given additional support by our spin-wave calculation in Sec. III.

Our cluster studies appear to argue against the speculation by Elser[6] that the double-peak feature in the Kagomé net heat capacity is a manifestation of a finite spin gap. According to that view the high-temperature peak corresponds to a condensation into a classical liquid of nearly degenerate singlet states formed by near-neighbor valence bonds. The low-temperature peak would then be the freezing of this classical liquid into a crystalline arrangement of valence bonds (spin-Peierls transition). The spin gap, or excitation energy from the ground state to the lowest state having higher total spin, as determined by our cluster studies seems to be quite small (see Table II). Even supposing this gap remains finite in the infinite system, its value is certainly much less than $\sim\frac{3}{4}J$ where the first peak occurs.

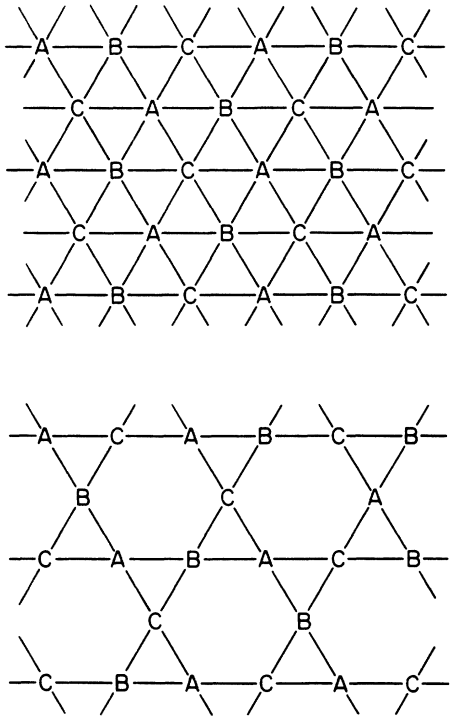

FIG. 4. Classical spin ordering on the triangular lattice and Kagomé net. A, B, C denote three-spin orientations with the property that the angle formed by any pair is 120°. One of the many classically degenerate ground-state structures is shown for the Kagomé net.

III. SPIN-WAVE CALCULATION

It has been proposed[13] that in low-spin antiferromagnets strong quantum fluctuations may generate a new kind of ground state without long-range order. The conventional spin-wave approximation has recently been applied to various types of two-dimensional quantum spin models with or without frustration[13,14] to address this issue. The zeroth-order approximation, corresponding to $S=\infty$ or classical spins, already displays a pathology in the Kagomé system. This is in sharp contrast to the triangular lattice system which we use as a comparison. First note that the minimum of the classical energy of three spins mutually coupled in a triangle is a planar configuration of spins with relative angles of 120°. Any state that achieves this local ordering in all triangles of the structure is a classical ground state. It is the solution of the global problem that distinguishes the Kagomé from triangular lattice systems (Fig. 4). In the latter, the local ordering at one triangle determines the ordering everywhere while in the Kagomé system there is a certain amount of freedom locally. This means that the zeroth-order spin-wave approximation is ill defined in the Kagomé system. A simple remedy is suggested by the triangular lattice itself: introduce two exchange constants J_1 and J_2 so that with $J_2=0$ one decouples one-quarter of the spins with the remainder coupled by J_1 in a Kagomé net. Keeping J_2 finite, the ordering at one triangle will select a unique global ordering as in the triangular lattice.

The Hamiltonian can be written in the following form:

$$H=J_1\sum_{\langle ij\rangle}\mathbf{S}_i\cdot\mathbf{S}_j+J_2\sum_{\langle ii'\rangle}\mathbf{S}_i\cdot\mathbf{S}_{i'}\ , \tag{3.1}$$

where the $\mathbf{S}_i$ are spin S operators and the assignment of J_1 and J_2 to the nearest-neighbor bonds of a triangular lattice is shown in Fig. 1.

Although with $J_2\neq0$ we now have a proper starting point for the calculation, the details of the calculation have become quite demanding. The Kagomé superstructure of the triangular lattice involves four spins in a unit cell while the $\sqrt{3}\times\sqrt{3}$ spin ordering involves three spins with the unfortunate consequence that to accommodate both a unit cell having 12 spins is required. This defines 12 sublattices denoted A_λ, B_λ, C_λ, D_λ where the subscript λ runs over 1, 2, and 3 (Fig. 1).

Following Jolicoeur and Le Guillou,[15] we choose the spins on the sublattices with subscript $\lambda=1$ (A_1,B_1,C_1, and D_1) to orient along the z direction, and those with subscript $\lambda=2$ and 3 rotated $-120°$ and 120° away from the z axis in the x-z plane. We then introduce 12 kinds of Holstein-Primakoff bosons, a_λ, b_λ, c_λ, and d_λ to describe the quantum fluctuations of the spins away from the classical directions. To leading order in $1/S$ the spin opera-

tors **S** on sublattice A_1 are parametrized as follows:

$$S^x_{A_1}=\frac{\sqrt{2S}}{2}(a_1^\dagger+a_1)\ ,$$
$$S^y_{A_1}=\frac{\sqrt{2S}}{2i}(a_1^\dagger-a_1)\ , \tag{3.2}$$
$$S^z_{A_1}=S-a_1^\dagger a_1\ .$$

The same formulas hold for sublattices B_1, C_1, and D_1 by replacing a_1 with b_1, etc. On the sublattices with $\lambda=2$ and 3, the three-spin components in (3.2) are rotated about the y axis by $-120°$ and 120°. As an example, we give the expression for the spin operators on sublattice A_2:

$$S^x_{A_2}=-\frac{\sqrt{3}}{2}(S-a_2^\dagger a_2)-\frac{\sqrt{2S}}{4}(a_2^\dagger+a_2)\ ,$$
$$S^y_{A_2}=\frac{\sqrt{2S}}{2i}(a_2-a_2^\dagger)\ , \tag{3.3}$$
$$S^z_{A_2}=-\tfrac{1}{2}(S-a_2^\dagger a_2)+\frac{\sqrt{3}}{2}\frac{\sqrt{2S}}{2}(a_2^\dagger+a_2)\ .$$

Substituting the above expressions back into the Hamiltonian (3.1) and expanding it, we obtain the Holstein-Primakoff oscillator Hamiltonian by keeping only the terms quadratic in the boson operators.

Each of the 12 kinds of Holstein-Primakoff bosons forms a triangular superlattice with lattice constant $2\sqrt{3}$. Since the coupling among these is translationally invariant with a unit cell of the same dimensions, we use the Fourier representation

$$a_1(\mathbf{r})=\frac{1}{\sqrt{N}}\sum_{\mathbf{k}\in\Lambda^*}a_1(\mathbf{k})e^{i\mathbf{k}\cdot\mathbf{r}}\ , \tag{3.4}$$

$$a_1(\mathbf{k})=\frac{1}{\sqrt{N}}\sum_{\mathbf{r}\in\Lambda}a_1(r)e^{-i\mathbf{k}\cdot\mathbf{r}}\ , \tag{3.5}$$

with similar expressions for other operators. In (3.4) and (3.5) we assume the system consists of $\sqrt{N}\times\sqrt{N}$ superlattice points Λ so that the set of **k**-space points Λ^* itself is a triangular lattice of N points within the Brillouin zone. Upon substituting (3.4) and (3.5) into the Holstein-Primakoff expression of the Hamiltonian, one obtains

$$H=H_0+H_2\ , \tag{3.6}$$

with

$$H_0=-9NS^2(J_1+J_2) \tag{3.7}$$

and

$$H_2=\tfrac{1}{2}SJ_1\sum_{\mathbf{k}}\left[|\tilde{\alpha}^\dagger(\mathbf{k}),\tilde{\beta}(\mathbf{k})|[\tilde{H}(\mathbf{k})]\begin{bmatrix}\tilde{\alpha}(\mathbf{k})\\ \tilde{\beta}^\dagger(\mathbf{k})\end{bmatrix}-18(1+\gamma)\right]\ , \tag{3.8}$$

where $\gamma=J_2/J_1$. The symbol $\tilde{\alpha}^\dagger(\mathbf{k})$ represents a row vector of 12 operators ordered as

$$\tilde{\alpha}^\dagger(\mathbf{k})=[\tilde{d}^\dagger(\mathbf{k}),\tilde{a}^\dagger(\mathbf{k}),\tilde{b}^\dagger(\mathbf{k}),\tilde{c}^\dagger(\mathbf{k})]\ , \tag{3.9}$$

where

$$\tilde{d}^\dagger(\mathbf{k})=[d_1^\dagger(\mathbf{k}),d_2^\dagger(\mathbf{k}),d_3^\dagger(\mathbf{k})] \tag{3.10}$$

and likewise for $\tilde{a}^\dagger(\mathbf{k})$, $\tilde{b}^\dagger(\mathbf{k})$, $\tilde{c}^\dagger(\mathbf{k})$. The Hermitian conjugates of these operators arranged in a column vector are denoted $\tilde{\alpha}(\mathbf{k})$ and $\tilde{\beta}(\mathbf{k})=\tilde{\alpha}(-\mathbf{k})$. The new Hamiltonian to be diagonalized is $\tilde{H}(\mathbf{k})$, a 24×24 matrix of the form

$$\tilde{H}(\mathbf{k})=\begin{bmatrix}M+K & -3K\\ -3K & M+K\end{bmatrix}_{(24\times24)}\ , \tag{3.11}$$

where

$$M=\begin{bmatrix}3\gamma I & 0 & 0 & 0\\ 0 & (2+\gamma)I & 0 & 0\\ 0 & 0 & (2+\gamma)I & 0\\ 0 & 0 & 0 & (2+\gamma)I\end{bmatrix}_{(12\times12)} \tag{3.12}$$

and

$$K=\begin{bmatrix}0 & \gamma J_1 & \gamma J_3 & \gamma J_2\\ \gamma J_1 & 0 & J_2 & J_3\\ \gamma J_3 & J_2 & 0 & J_1\\ \gamma J_2 & J_3 & J_1 & 0\end{bmatrix}_{(12\times12)}\ . \tag{3.13}$$

In these formulas, I is the 3×3 identity matrix and

$$J_i=\begin{bmatrix}0 & x_i^* & x_i\\ x_i & 0 & x_i^*\\ x_i^* & x_i & 0\end{bmatrix}_{(3\times3)}\ , \tag{3.14}$$

with

$$x_j=\tfrac{1}{4}e^{-i\mathbf{k}\cdot\mathbf{r}_j},\quad j=1,2,3\ , \tag{3.15}$$
$$\mathbf{r}_1=(0,1)\ ,$$
$$\mathbf{r}_2=(-\sqrt{3}/2,-\tfrac{1}{2})\ , \tag{3.16}$$
$$\mathbf{r}_3=(\sqrt{3}/2,-\tfrac{1}{2})\ .$$

Following Jolicoeur and Le Guillou,[15] we consider the generalized Bogoliubov transform matrix T as follows:[16]

$$\begin{bmatrix}\mathcal{A}(\mathbf{k})\\ \mathcal{B}^\dagger(\mathbf{k})\end{bmatrix}=T\begin{bmatrix}\tilde{\alpha}(\mathbf{k})\\ \beta^\dagger(\mathbf{k})\end{bmatrix}\ , \tag{3.17}$$

where $\mathcal{A}(\mathbf{k})$ is a column vector with 12 components $\mathcal{A}_n(\mathbf{k})$ $(n=1,2,\ldots,12)$ and likewise for $\mathcal{B}^\dagger(\mathbf{k})$. To preserve the bosonic commutation relations, T has to satisfy

$$T^{-1}=\eta T\eta\ , \tag{3.18}$$

where

$$\eta=\begin{bmatrix}I & 0\\ 0 & -I\end{bmatrix}_{(24\times24)} \tag{3.19}$$

and I is now the 12×12 identity matrix. Substituting (3.17) and (3.18) back into (3.8) we have

$$H_2=\tfrac{1}{2}SJ_1\sum_{\mathbf{k}}\left[[\mathcal{A}^\dagger(\mathbf{k}),\mathcal{B}(\mathbf{k})]\eta T[\eta\tilde{H}(\mathbf{k})]T^{-1}\begin{bmatrix}\mathcal{A}(\mathbf{k})\\ \mathcal{B}^\dagger(\mathbf{k})\end{bmatrix}-18(1+\gamma)\right]. \tag{3.20}$$

To obtain a diagonal form for H_2, an appropriate choice for T is[16]

$$T^{-1}=(V^1\cdots V^{12}W^1\cdots W^{12})_{(24\times 24)}, \tag{3.21}$$

where V^n and W^n are the eigenvectors of $\eta\tilde{H}(\mathbf{k})$ with corresponding eigenvalues $(\omega_n,-\omega_n)$ where we have used the fact that the eigenvalues of $\eta\tilde{H}(\mathbf{k})$ occur in pairs and set $\omega_n>0$.

Expressed in terms of normal modes $\mathcal{A}_n$, the Hamiltonian becomes

$$H=H_0+\tfrac{1}{2}SJ_1\sum_{\mathbf{k}}\left[2\sum_{n=1}^{12}(\omega_n+\tfrac{1}{2})\mathcal{A}_n^\dagger\mathcal{A}_n-18(1+\gamma)\right], \tag{3.22}$$

with ground-state energy

$$E_0=-9NS^2(J_1+J_2)+\tfrac{1}{2}SJ_1\sum_{\mathbf{k}}\left[\sum_{n=1}^{12}\omega_n-18(1+\gamma)\right]. \tag{3.23}$$

The ground-state expectation value of the operator

$$M^z_{A_1}=SN-\sum_{\mathbf{k}}a_1^\dagger(\mathbf{k})a_1(\mathbf{k}) \tag{3.24}$$

gives the ground-state staggered magnetization on sublattice A_1,

$$\langle M^z_{A_1}\rangle=SN-\sum_{\mathbf{k}}\sum_{n=1}^{12}|W_4^n|^2, \tag{3.25}$$

where subscript 4 means the fourth row element of the vector W^n and comes from our definition of $\tilde{\alpha}^\dagger(\mathbf{k})$.

The diagonalization of the non-Hermitian 24×24 matrix $\eta\tilde{H}(\mathbf{k})$ is the nontrivial part of this calculation. The problem can be simplified following the observation by Jolicoeur and Le Guillou[15] that the J_i can be diagonalized simultaneously. The eigenvectors v_1, v_2, and v_3 and the corresponding eigenvalues ρ_1, ρ_2, and ρ_3 of J_i are

$$v_1=\begin{bmatrix}1\\1\\1\end{bmatrix},\quad v_2=\begin{bmatrix}1\\\omega\\\omega^2\end{bmatrix},\quad v_3=\begin{bmatrix}1\\\omega^2\\\omega\end{bmatrix}, \tag{3.26}$$

$$\begin{aligned}\rho_1(x_i)&=x_i^*+x_i,\\ \rho_2(x_i)&=\omega x_i^*+\omega^2 x_i,\\ \rho_3(x_i)&=\omega^2 x_i^*+\omega x_i,\end{aligned} \tag{3.27}$$

where $\omega=e^{-i2\pi/3}$. The eigenvalue problem of $\eta\tilde{H}(\mathbf{k})$ thus reduces to that of three smaller matrices of the form

$$\begin{bmatrix}3\gamma P & \gamma\rho_i(x_1)Q & \gamma\rho_i(x_3)Q & \gamma\rho_i(x_2)Q\\ \gamma\rho_i(x_1)Q & (2+\gamma)P & \rho_i(x_2)Q & \rho_i(x_3)Q\\ \gamma\rho_i(x_3)Q & \rho_i(x_2)Q & (2+\gamma)P & \rho_i(x_1)Q\\ \gamma\rho_i(x_2)Q & \rho_i(x_3)Q & \rho_i(x_1)Q & (2+\gamma)P\end{bmatrix}_{(8\times 8)},\quad i=1,2,3, \tag{3.28}$$

where

$$P=\begin{bmatrix}1 & 0\\ 0 & -1\end{bmatrix},\quad Q=\begin{bmatrix}1 & -3\\ 3 & -1\end{bmatrix}. \tag{3.29}$$

Each of the three matrices still preserves the eigenvalue-pair property. Keeping this in mind and noticing that P^2, Q^2, PQ, and QP all commute among one another, we can square (3.28) to simplify the eigenvalue problem further. The following conclusion is obtained after those manipulations: ω_n^2 are the eigenvalues of three 4×4 matrices,

$$\begin{bmatrix}a & a_1+c_1 & a_3+c_3 & a_2+c_2\\ -a_1+c_1 & d_1 & b_2 & b_3\\ -a_3+c_3 & b_2 & d_3 & b_1\\ -a_2+c_2 & b_3 & b_1 & d_2\end{bmatrix}, \tag{3.30}$$

where

$$\begin{aligned}a&=9\gamma^2-8\gamma^2[\rho_i^2(x_1)+\rho_i^2(x_2)+\rho_i^2(x_3)],\\ a_1&=6(1-\gamma)\gamma\rho_i(x_1),\\ b_1&=2(2+\gamma)\rho_i(x_1)-8(1+\gamma^2)\rho_i(x_2)\rho_i(x_3),\\ c_1&=(4\gamma^2+2\gamma)\rho_i(x_1)-16\rho_i(x_2)\rho_i(x_3),\\ d_1&=(2+\gamma)^2+8(1-\gamma^2)\rho_i^2(x_1)\\ &\quad-8[\rho_i^2(x_1)+\rho_i^2(x_2)+\rho_i^2(x_3)],\end{aligned} \tag{3.31}$$

and other entries of the above matrix (3.30) can be evaluated by cyclically permuting the subscripts 1,2,3.

Because of the complexity of these 4×4 matrices, the final diagonalization of (3.28) is carried out numerically and V and W are obtained by the inverse iterative power method. For the triangular lattice ($\gamma=1$), the ground-state energy and ground-state sublattice magnetization given by Jolicoeur and Le Guillou[15] are recovered as a test of our programs. In Fig. 5 we plot the locus of points

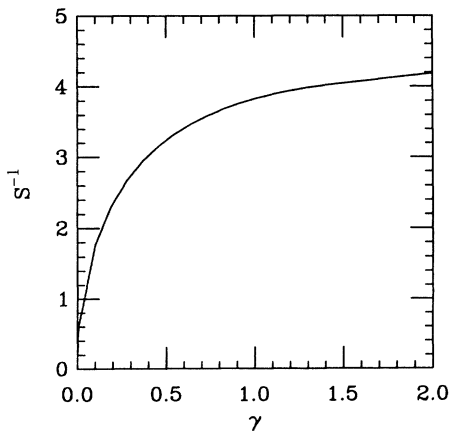

FIG. 5. Phase diagram of the triangular lattice HAF with exchange constants J_1 and J_2. The solid line shows where the sublattice magnetization is zero as calculated in the spin-wave approximation.

in the (S,γ) " phase diagram" where the sublattice magnetization $M^z_{A_1}$ vanishes as calculated above in the lowest spin-wave approximation. Below the solid curve (phase boundary) $M^z_{A_1}\neq 0$ and the system has long-range $\sqrt{3}\times\sqrt{3}$ spin ordering. Above the curve the sublattice magnetization is presumed to be destroyed by quantum fluctuations and the spins are said to be "disordered." Evidently there exists a finite region near $\gamma=0$ where the ground state is disordered even for large spins. For the case of physical interest, $S=\frac{1}{2}$, the transition from an ordered to a disordered ground state occurs at $\gamma\sim 0.2$. The divergence of quantum fluctuations as $\gamma\rightarrow 0$ (making even the large spin system unstable) is similar to what was found by Chandra and Doucot[14] for the case of the square-lattice HAF with competing nearest- and next-nearest-neighbor interactions. Shown in Fig. 6 are the dispersion relations for the 12 spin-wave modes $\mathcal{A}_n$. The growth of the quantum fluctuations which destroy spin ordering can be associated with the softening of half of these modes as $\gamma\rightarrow 0$.

IV. DECOUPLED-CELL MONTE CARLO SIMULATION

The double peak in the nuclear spin heat capacity is a distinctive property of the ^{3}He second layer and one that presents a significant challenge to theoretical models. Although a double peak was found in a numerical calculation for the present model on a 12-site cluster,[6] we do not accept this as strong evidence. For example, one might worry that the low temperature of the second peak ($\simeq 0.1J/k_B$) merely reflects a subtle form of frustration when the magnetic unit cell of the ground state does not agree with the dimensions of the cluster. The same criticism applies to the calculation of Roger[7] using a different model but a cluster of essentially the same size. In this section we present a study of the thermodynamics of our model in the Kagomé limit ($J_2=0$) using the decoupled-cell Monte Carlo method (DCMC) introduced by Homma *et al.*[9] This method also suffers from finite-size limitations but we feel these limitations are signficantly different so as to complement the previous study.

The DCMC is very appealing for the Kagomé net be-

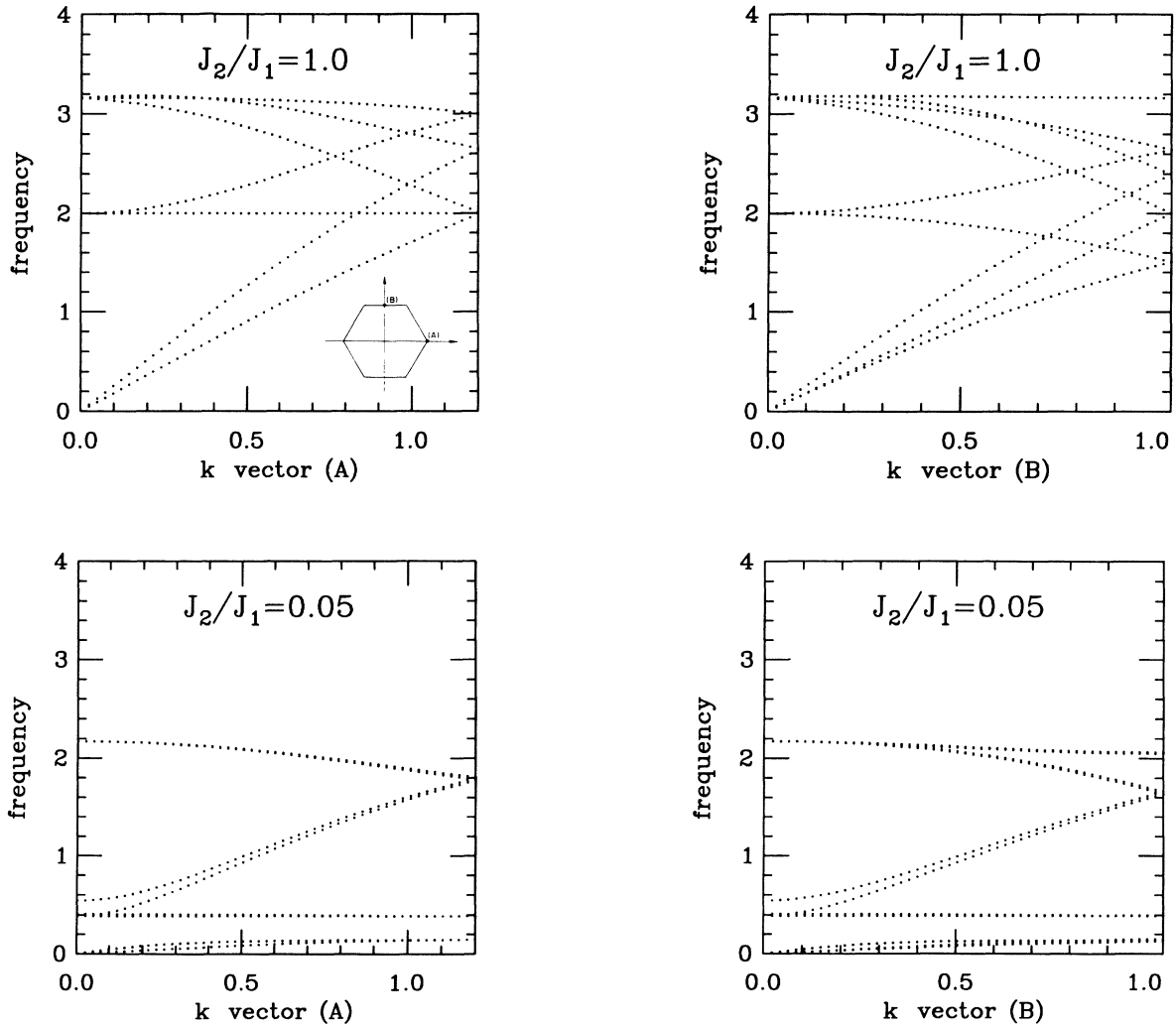

FIG. 6. Dispersion relations of magnons along directions A and B in the first Brillouin zone.

cause of the possibility of having relatively large decoupled cells. We begin with a description of the core of the DCMC algorithm. The canonical ensemble of a quantum spin-$\frac{1}{2}$ system can be generated by the time sequence of a Markov chain whose transition probability for single-spin-flip $W(\sigma_i \to -\sigma_i)$ satisfies the detailed-balance principle. One of the commonly chosen forms of the transition probability is the Metropolis function:

$$W(\sigma_i \to -\sigma_i) = \max\left\{1, \frac{\langle \cdots -\sigma_i \cdots | e^{-\beta H} | \cdots -\sigma_i \cdots \rangle}{\langle \cdots \sigma_i \cdots | e^{-\beta H} | \cdots \sigma_i \cdots \rangle}\right\}, \tag{4.1}$$

where $|\cdots \sigma_i \cdots\rangle$ denotes the spin configuration of the whole system and, $S_i^z = \sigma_i$, and $\beta = (k_B T)^{-1}$. The DCMC algorithm approximates W in (4.1) by W_{DC} defined as the following:

$$W(\sigma_i \to -\sigma_i) \simeq W_{\mathrm{DC}}(\sigma_i \to -\sigma_i) = \max\left\{1, \frac{\langle \cdots -\sigma_i \cdots | e^{-\beta H(\nu,i)} | \cdots -\sigma_i \cdots \rangle}{\langle \cdots \sigma_i \cdots | e^{-\beta H(\nu,i)} | \cdots \sigma_i \cdots \rangle}\right\}, \tag{4.2}$$

where $H(\nu,i)$ is the restriction of the Hamiltonian H to a finite neighborhood ν about spin i (the decoupled cell). Once the transition probabilities W_{DC} are obtained, the algorithm can be implemented as a classical Monte Carlo simulation. In practice, transition probabilities W_{DC} in (4.2) are obtained by exactly solving the eigenvalue problem of Hamiltonian $H(\nu,i)$ and stored before the main Monte Carlo simulation.

In the Ising limit of our Hamiltonian, the DCMC algorithm is exact already when ν consists of spin i and its near neighbors. When the off-diagonal couplings are turned on, it is believed that the dependence of the transition probabilities on the spin configurations outside the decoupled cell becomes less and less significant as the cell size increases, particularly at higher temperatures. At lower temperatures, in analogy with the growth of the thermal de Broglie wavelength of a particle, one expects that larger cells are needed to capture the correlations that determine W_{DC}. While we do not know the scaling of cell size with temperature, we feel safe in using the following empirical rule: follow the behavior of a thermodynamic function down to the same low temperature using one size of decoupled cell and repeat using a cell that is slightly larger. The point where the two functions deviate is then the lowest temperature for which the simulation results are reliable.

We have performed the DCMC simulations on decoupled cells with 5, 11, and 13 spins (Fig. 7). These decoupled cells will be referred to as $c(5)$, $c(11)$, and $c(13)$. Using only block diagonalization by the total z component of spin we were able to construct the Hamiltonian matrix $H(\nu,i)$ and evaluated the transition probabilities in (4.2) without utilizing any other symmetries for the

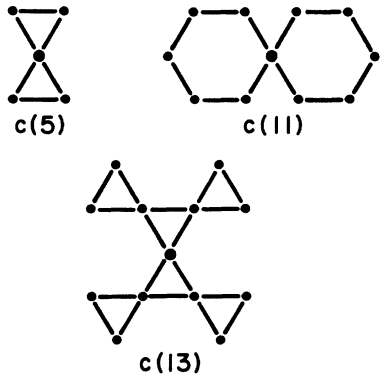

FIG. 7. Decoupled cells $c(5)$, $c(11)$, and $c(13)$.

smallest decoupled cells. For $c(13)$ we were forced to consider additional symmetries because of memory limitations. While the translational symmetries no longer exist because of the free boundary, the Hamiltonian $H(\nu,i)$ is invariant under the exchange of the outermost spins within each of the outermost triangles. Utilizing all the 16 symmetry elements, the rank of the largest Hamiltonian matrix to be diagonalized is reduced to 494. The computation of the transition probabilities in (4.2) for 40 different temperature values takes about 10 h on the Sun SparcStation1.

The internal energy and heat capacity were computed with different decoupled cells for a Kagomé net of $8\times8\times3$ spins having periodic boundary conditions. Whereas the internal energy,

$$\varepsilon = \frac{3J}{N} \sum_{\langle ij \rangle} \langle S_i^z \cdot S_j^z \rangle \tag{4.3}$$

can be measured directly, the heat capacity which involves off-diagonal operators $[H^2 \propto \cdots (S_i^z \cdot S_j^z)(S_{i'}^x \cdot S_{j'}^x) \cdots]$ cannot since the DCMC

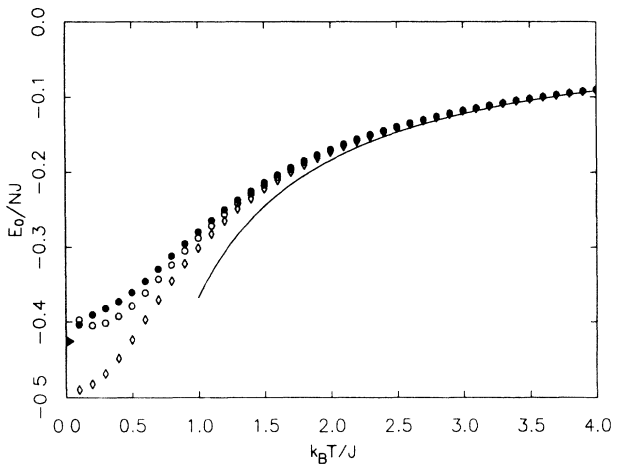

FIG. 8. Internal energy per spin vs temperature of a spin-$\frac{1}{2}$ Kagomé HAF. The symbols ($\Diamond$), ($\circ$), and ($\bullet$) are DCMC results obtained from decoupled cells $c(5)$, $c(11)$, and $c(13)$, respectively. The solid line shows the lowest-order term of the high-temperature expansion. The mark on the energy axis corresponds to the ground-state energy of the Kagomé net obtained by direct diagonalization.

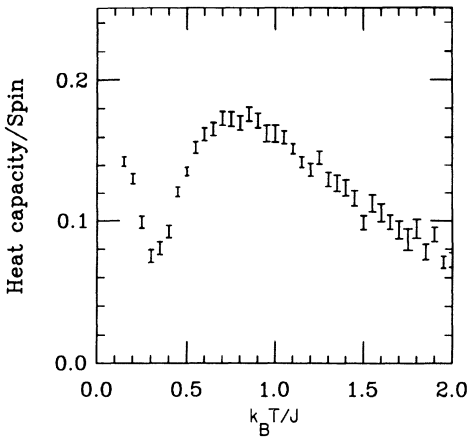

FIG. 9. Heat capacity per spin (in units of k_B) as a function of temperature from $c(13)$.

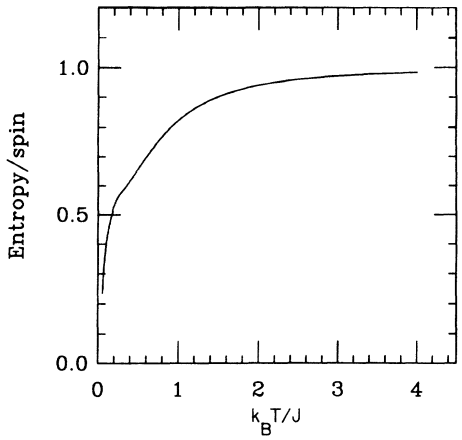

FIG. 10. Entropy per spin (in units of $k_B\ln 2$) as a function of temperature from $c(13)$.

method only generates diagonal elements of the density matrix. Nevertheless, the heat capacity can be computed using finite differences of energy measurements,

$$c=\frac{\Delta\varepsilon}{\Delta T}\ . \tag{4.4}$$

We have used 100 000 Monte Carlo steps per spin, divided into 20 groups to estimate the statistical errors. This main part of the simulation also takes about 10 hours.

In the high-temperature regime, the internal energy obtained from different decoupled cells is in good agreement as expected (Fig. 8). Agreement with the first term in the high-temperature expansion, $\varepsilon=-0.375\beta J^2$, is also quite good. Towards the low-temperature regime, the situation becomes more intriguing. The simulation with $c(5)$ behaves like the corresponding Ising problem in that the internal energy extrapolates to a value close to $-0.5J$ per spin. The internal energies of the larger cells $c(11)$ and $c(13)$ are substantially shifted up with respect to $c(5)$ at low temperatures. A clear sign that the validity of the DCMC method fails at low enough temperatures is seen from the fact that the internal energy of $c(11)$ actually turns up slightly. The same behavior was observed by Homma *et al.*[9] on a one-dimensional HAF chain. To our delight, this pathology of the method is corrected by $c(13)$. This, our largest cell, rather than showing a minimum in the energy has a monotonic behavior with an inflection point. Below the inflection point the downturn in the energy even offers hope that at $T=0$ it will be close to the value $-0.434J$ determined by the exact diagonalization studies in Sec. I. Clearly larger cells are needed to study this very-low-temperature region. Nevertheless, we believe that we have achieved reasonable convergence down to temperatures near this inflection point and it is really only this part that is responsible for the first maximum in the heat capacity.

The heat capacity calculated with $c(13)$ is plotted in Fig. 9. Clearly, besides the first peak located at about $T=0.75J/k_B$, a second peak emerges when the temperature drops below $0.3J/k_B$. The location of the second peak can roughly be estimated at $T=0.1J/k_B$. These results for the heat capacity match those of the earlier study[6] excellently, i.e., both in the location of the peaks and their heights. Although the agreement in the low-temperature peak may be fortuitous we believe now that the high-temperature peak is an intrinsic property of the model. A plot of the entropy in Fig. 10 shows that the entropy below this peak is in rough agreement with the value determined by Greywall and Busch.[4]

V. CONCLUSION

Our numerical studies of the HAF on a Kagomé net have revealed two things: (1) the likely absence of spin ordering in the ground state and (2) a double peak in the heat capacity. Moreover, our spin-wave calculation for the triangular lattice with exchange constants J_1 and J_2 suggested the possibility of two zero-temperature phases where the phase corresponding to the Kagomé limit, $\gamma=J_2/J_1\rightarrow 0$, has disordered spins. Thus we speculate that a double-peaked heat capacity is a characteristic property of the J_1/J_2 triangular lattice system, provided that $\gamma<0.2$. We do not have a precise picture of the form of condensation responsible for the high-temperature peak. The burden of demonstrating that the present model describes the absorbed ^{3}He system has now shifted to the microscopic origins of exchange. Besides the need to have biquadratic spin terms (from four- and higher-order cycles) negligible it is necessary that the combined contributions of pair and three-cycle exchange either are small for J_2 or nearly cancel.

ACKNOWLEDGMENTS

One of us (C.Z.) would like to thank J. B. Marston, K. Runge, and T. Basile for very useful discussions. The financial support for C. Z. was provided by National Science Foundation (NSF) Grant No. DMR-88-18558. The other (V.E.) was supported by the Cornell University Materials Science Center, Alfred P. Sloan Foundation, AT&T Bell Laboratories, the David and Lucile Packard Foundation, and the NSF Grant No. DMR-89-58510.

[1]H. Godfrin, R. R. Ruel, and D. D.Osheroff, Phys. Rev. Lett. **60**, 305 (1988).
[2]H. Franco, R. E. Rapp, and H. Godfrin, Phys. Rev. Lett. **57**, 1161 (1986).
[3]C. Tiby, H. Wiechert, H. J. Lauter, and H. Godfrin, Physica B+C (Amsterdam) **107C**, 209 (1981).
[4]D. S. Greywall and P. A. Busch, Phys. Rev. Lett. **62**, 1868 (1989).
[5]S. W. Van Sciver and O. E. Vilches, Phys. Rev. B **18**, 285 (1978).
[6]V. Elser, Phys. Rev. Lett. **62**, 2405 (1989).
[7]M. Roger, Phys. Rev. Lett. **64**, 297 (1990).
[8]K. Machida and M. Fujita, Phys. Rev. B **42**, 2673 (1990).
[9]S. Homma, K. Sano, H. Matsuda, and N. Ogita, Prog. Theor. Phys. Suppl. **87**, 127 (1986).
[10]S. Fujiki and D. D. Betts, Can. J. Phys. **64**, 876 (1986).
[11]S. Fujiki and D. D. Betts, Can. J. Phys. **65**, 76 (1987).
[12]H. Nishimori and H. Nakanishi, J. Phys. Soc. Jpn. **57**, 626 (1988).
[13]P. W. Anderson, Phys. Rev. **86**, 694 (1964).
[14]P. Chandra and B. Doucot, Phys. Rev. B **38**, 9335 (1989).
[15]Th. Jolicoeur and J. C. Guillou, Phys. Rev. B **40**, 2727 (1989).
[16]Jean-Paul Blaizot and G. Ripka, *Quantum Theory of Finite Systems* (MIT Press, Cambridge, MA, 1986), Chap. 4.